NANO LETTERS

pubs.acs.org/NanoLett

Letter

Bright and Near-Unity Polarized Light Emission Enabled by Highly Luminescent Cu_2I_2-Dimer Cluster-Based Hybrid Materials

Jing-Jing Wang,[†] Xiaoyu Mao,[†] Jun-Nan Yang, Yi-Chen Yin, Ji-Song Yao, Li-Zhe Feng, Feng Zhu, Cheng Ma, Cui Yang, Gang Zou, Guozhen Zhang,* Hualing Zeng,* and Hong-Bin Yao*

Cite This: *Nano Lett.* 2021, 21, 4115–4121

Read Online

ACCESS | Metrics & More | Article Recommendations | Supporting Information

ABSTRACT: As one fundamental property of light, polarization has a huge impact in quantum optics and optoelectronics through light–matter interactions. However, the bright and near-unity polarized light emissions in the visible range by solid crystalline materials are scantly realized. Here, we report well-defined quasi two-dimensional (2D) hybrid crystals based on the linear alignment of Cu_2I_2-dimer/bidentate ligand hybrid clusters for achieving bright and near-unity linearly polarized light emissions. Using first-principle calculations, we demonstrate that the superaligned transition dipole moments are the key for the observed excellent polarized light emissions. To further enhance the photoluminescence (PL) polarization degree, we fabricate Cu_2I_2-dimer-based hybrid nanobelts, which display high PL quantum yield (up to 64%) and ultrahigh PL polarization degree (~0.99). Our reported copper iodine cluster-based luminescent hybrid materials for bright and highly polarized light emissions will have great potential for future quantum optics applications.

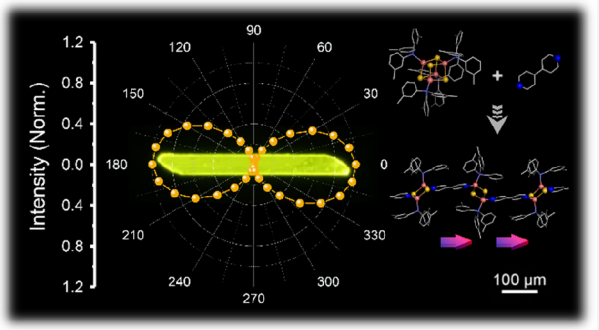

KEYWORDS: *Cu–I hybrid cluster, photoluminescence, linear polarization, transition dipole moment*

The brightness of linearly polarized light generated from a polarizer suffers great intensity loss, which greatly hinders the applications for advanced display, quantum information, and bioimaging, to name a few. The polarized light emissions directly obtained from photoluminescent materials either with coherent electronic quantum states[1−3] or with highly anisotropic structures[1,4−6] are promising to avoid the intensity loss. However, limited by the inherent fast spin decoherence in most solid-state crystals, it is rather challenging to realize linearly polarized light emissions via the electronic state quantum control at room temperature.[7−9] As an alternative efficient pathway, the polarized light emissions originating from structure anisotropy present an attractive feasibility. The luminescent materials with anisotropic nanostructure such as InP nanowire,[4] CdSe nanowire,[10] $CsPbBr_3$ nanocrystals,[11,12] 2D-(In, Ga)N/GaN quantum wells[13] and monolayer black phosphorus[1] have been shown to display linearly polarized light emissions. Nevertheless, up to now, the highest linear polarization degree observed in these materials is 0.96,[4,13] meaning it has not yet reached complete polarization.

Specific to photoluminescent materials with structural anisotropy, besides the nanostructured effect, the linear polarization degree of the PL is essentially determined by the optical transition (electric) dipole moments in the crystals.[5,14] In the past decades, the polarized PL emissions have been demonstrated in the anisotropic packing of chromophores in the polymer fibers,[14,15] metal organic frameworks[16] and organometallic crystals,[5] but only displayed low polarization degree less than 0.9. This is rooted in the disordered distribution nature of the transition dipole moments in these reported PL crystalline materials, which allows for unidirectional electromagnetic oscillations (Figure 1a). To that end, a perfect alignment of the transition dipole moments in one direction should be ensured in photoluminescent materials.

The superalignment of all the optical transition dipole moments in a fixed direction without any deviation can yield completely polarized PL emissions (Figure 1b). However, it is very challenging to enforce uniform orientation of all transition dipole moments, which can be significantly affected by the steric hindrance of molecular packing, molecular vibrations, and material defects. For instance, even in one-dimensional photoluminescent polymers where the structure anisotropy is extremely high as a result of dimensionality, the polarization degree of the PL is still lower than 0.9 because of the influence

Received: March 21, 2021
Revised: April 15, 2021
Published: April 22, 2021

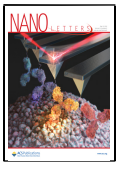

https://doi.org/10.1021/acs.nanolett.1c01149
Nano Lett. 2021, 21, 4115–4121

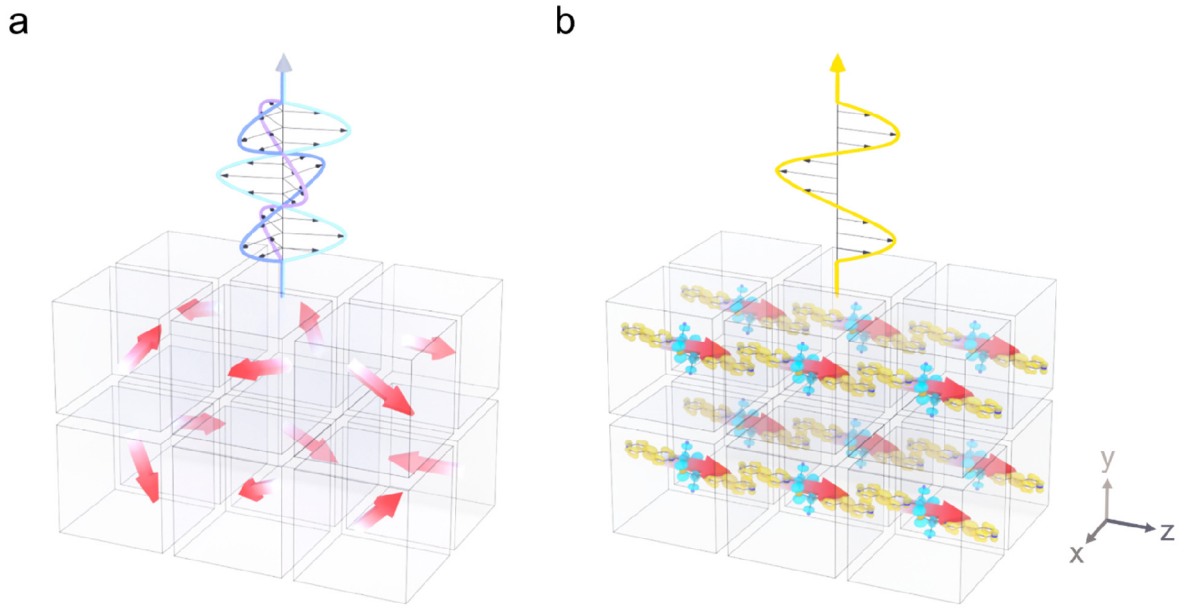

Figure 1. (a) Schematic illustration of the randomly oriented transition dipole moments and the correlated low polarization degree of PL emission. (b) Ideal model with oriented transition dipole moments and the locked orientation that yield completely polarized PL.

of depolarization interaction from the dielectric surroundings.[14−16]

Herein, we report, for the first time, that a bright PL with near-unity linear polarization degree can be achieved in a copper-iodide-dimer (Cu_2I_2)/bidentate organic ligand hybrid crystal by locking the linearly aligned transition dipole moments via hybrid crystal engineering. We build up Cu_2I_2/bidentate-ligand hybrid crystals with purposeful manipulation of optical dipoles via the charge transfer between Cu_2I_2 and organic ligands.[17,18] It is worth mentioning that despite various copper-iodide/organic ligand hybrid photoluminescent materials with high photoluminescence quantum yields (PLQYs) having been intensively explored as solid phosphor powders,[19−22] the elaborate manipulation on the PL polarization property of copper-iodide/organic ligand hybrid clusters has not been reported yet.

We employed a facile two-layer diffusion single-crystal growth approach to implement the crystal engineering of Cu_2I_2/bidentate-ligand hybrid clusters (Figure 2a). The Cu_4I_4[P-(m-Tol)$_3$]$_4$(P-(m-Tol)$_3$:tris(3-methylphenyl) phosphine) clusters were used as initial building blocks because of their high solubility in chloroform.[19] The Cu_4I_4[P-(m-Tol)$_3$]$_4$/chloroform solution was loaded into a reaction vial as a bottom layer and then the dimethyl sulfoxide/ethanol solution containing organic bidentate ligands was added and served as a top layer. These two separated layers enable the slow diffusion and thorough interaction of Cu_4I_4[P-(m-Tol)$_3$]$_4$ clusters and bidentate ligands, which facilitates the growth of high-quality hybrid crystals. The Cu_4I_4[P-(m-Tol)$_3$]$_4$ cluster experienced a structural change to the Cu_2I_2-dimer with the break of Cu−I bonds and the connection with organic ligands to form the anisotropic Cu_2I_2-bidentate hybrid chains. It is anticipated that the hybrid chains surrounded by large-sized P-(m-Tol)$_3$ groups prefer to stack with each other in a highly parallel direction. Four bidentate ligands (pyrimidine, pyrazine, 3,3′-bipyridine, and 4,4′-bipyridine, abbreviated as pym, pyz, 3,3′-bpy, and 4,4′-bpy, respectively) were used to successfully fabricate four types of high-quality hybrid crystals (Figure 2b−e) via this two-layer diffusion process.

The structures of the obtained hybrid crystals were resolved by single-crystal X-ray diffraction (SCXRD) (Table S1 and crystallographic information files) and the chemical formulas were determined to be Cu_2I_2[P-(m-Tol)$_3$]$_2$(pym)$_2$, Cu_2I_2[P-(m-Tol)$_3$]$_2$(pyz), Cu_2I_2[P-(m-Tol)$_3$]$_2$(3,3′-bpy), and Cu_2I_2[P-(m-Tol)$_3$]$_2$(4,4′-bpy), (abbreviated as **Cu_2I_2-pym**, **Cu_2I_2-pyz**, **Cu_2I_2-3,3′-bpy**, and **Cu_2I_2-4,4′-bpy**), respectively (Figures S1−S4). We analyzed the packing style of different Cu_2I_2-bidentate hybrid clusters in the obtained crystals to illustrate the ligand effect on the structure engineering. Although all Cu_2I_2-bidentate clusters display the trend in anisotropic alignment, the uniformity of their orientation is significantly influenced by the steric hindrance effect of ligands (Figure 2b−e and Figure S5). It is very intriguing that **Cu_2I_2-3,3′-bpy** and **Cu_2I_2-4,4′-bpy** hybrid chains are horizontally arranged in parallel with each other in (001) and (010) planes, respectively, further forming quasi-2D layered structures with enhanced thermal stabilities (Figures S6−S8). We carried out density functional theory (DFT) calculations to reveal the charge transfer in the hybrid crystals for PL emissions. We found that the valence band maximum (VBM) region mostly consists of the atom states of inorganic Cu_2I_2 components (Cu 3d and I 5p orbitals), and the conduction band minimum (CBM) is composed dominantly of the atom states of the organic N-heterocycles ligands (C and N 2p orbitals) (Figure 2b−e and Figure S9). Therefore, upon light exposure, the photo excitation and emission process between VBM and CBM involves charge transfer between Cu_2I_2 dimers and bidentate ligands, which indicates a halide to ligand charge transfer (XLCT) or metal to ligand charge transfer (MLCT) (or a combination) mechanism with phosphorescent emission for such hybrid luminescent materials (Figure S10). As the emission energies suggest a major correlation with the constituent organic ligands, the different choice of organic ligands will consequently modulate the PL emissions of hybrid crystals by tailoring their band gaps. As a result, all hybrid

https://doi.org/10.1021/acs.nanolett.1c01149
Nano Lett. 2021, 21, 4115−4121

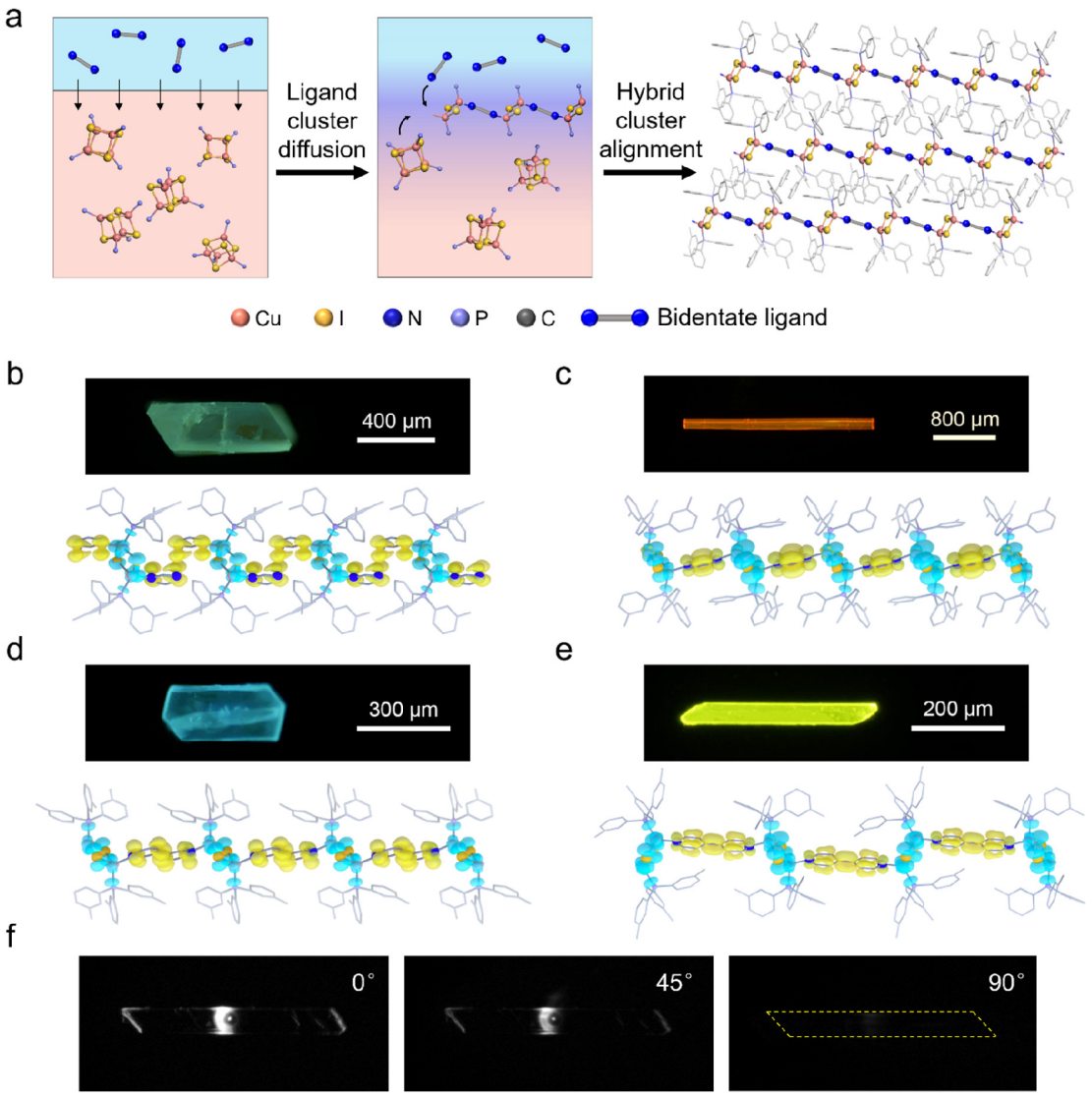

Figure 2. (a) Schematic illustration of the proposed two-layer diffusion model for the hybrid single-crystal growth. The 3-methylphenyl on the P-(m-Tol)$_3$ ligands are omitted for clarity. (b–e) Fluorescence microscope images and packing structure models of **Cu_2I_2-pym**, **Cu_2I_2-pyz**, **Cu_2I_2-3,3′-bpy**, and **Cu_2I_2-4,4′-bpy** microcrystals, respectively. All hydrogen atoms are omitted for clarity. VBM (cyan) and CBM (yellow) are collected in a single model for better visualizing the charge transfer nature of the electronic transition involved in PL. (f) The gray-color light emission image of the **Cu_2I_2-4,4′-bpy** microcrystal under the excitation of a focused laser beam (λ_{ex} = 450 nm) through a linear polarizer at different angles to the crystal orientation.

crystals exhibit strong PL at room temperature with emission colors spanning almost the entire visible region and high PLQY values ranging from 54 to 84% (Figure 2b–e and Figure S11). Typically, the parallel arrangement of hybrid clusters can generate a uniformly oriented spatial distribution of the transition dipole moments, which implies a potential PL polarization nature of all types of hybrid crystals. Among them, we chose the **Cu_2I_2-4,4′-bpy** microcrystal as a representative to visually investigate the PL polarization characteristic by a homemade setup. (Figure S12). Interestingly, the obtained hybrid crystal basically exhibited optical waveguide behavior ascribed to the obvious PL spots detected at the tip site when excited by a laser beam of 450 nm. Particularly, as shown in Figure 2f, when the polarizer was rotated to different angles relative to the hybrid crystal, significant PL brightness variation occurred at both the excitation site and the tip site, which preliminary evidenced a linear-polarized PL characteristic and a good polarization retention along the optical propagation process in the hybrid crystal.

To further confirm the polarized PL, we measured the linear polarization degree of the PL from four kinds of hybrid crystals by a homemade instrument (Figure S13, Supporting Information). Notably, the PL polarization degree of **Cu_2I_2-3,3′-bpy** (0.851) and **Cu_2I_2-4,4′-bpy** (0.965) hybrid crystals are both much higher than that of **Cu_2I_2-pym** (0.775) and **Cu_2I_2-pyz** (0.741) crystals (Figure 3a–d). The results imply the alignment of transition dipole moments in Cu-bidentate ligand quasi-2D crystal plane is vital for the linearly polarized PL emissions. We then computed the corresponding transition dipole moments in **Cu_2I_2-3,3′-bpy** and **Cu_2I_2-4,4′-bpy** hybrid cluster models which are extracted from their single crystal structures using time-dependent DFT (TDDFT) method to investigate the relationship between the PL polarization degree and the orientation of transition dipole moments (Table S2). The calculation results reveal that the spatial distribution of

https://doi.org/10.1021/acs.nanolett.1c01149
Nano Lett. 2021, 21, 4115–4121

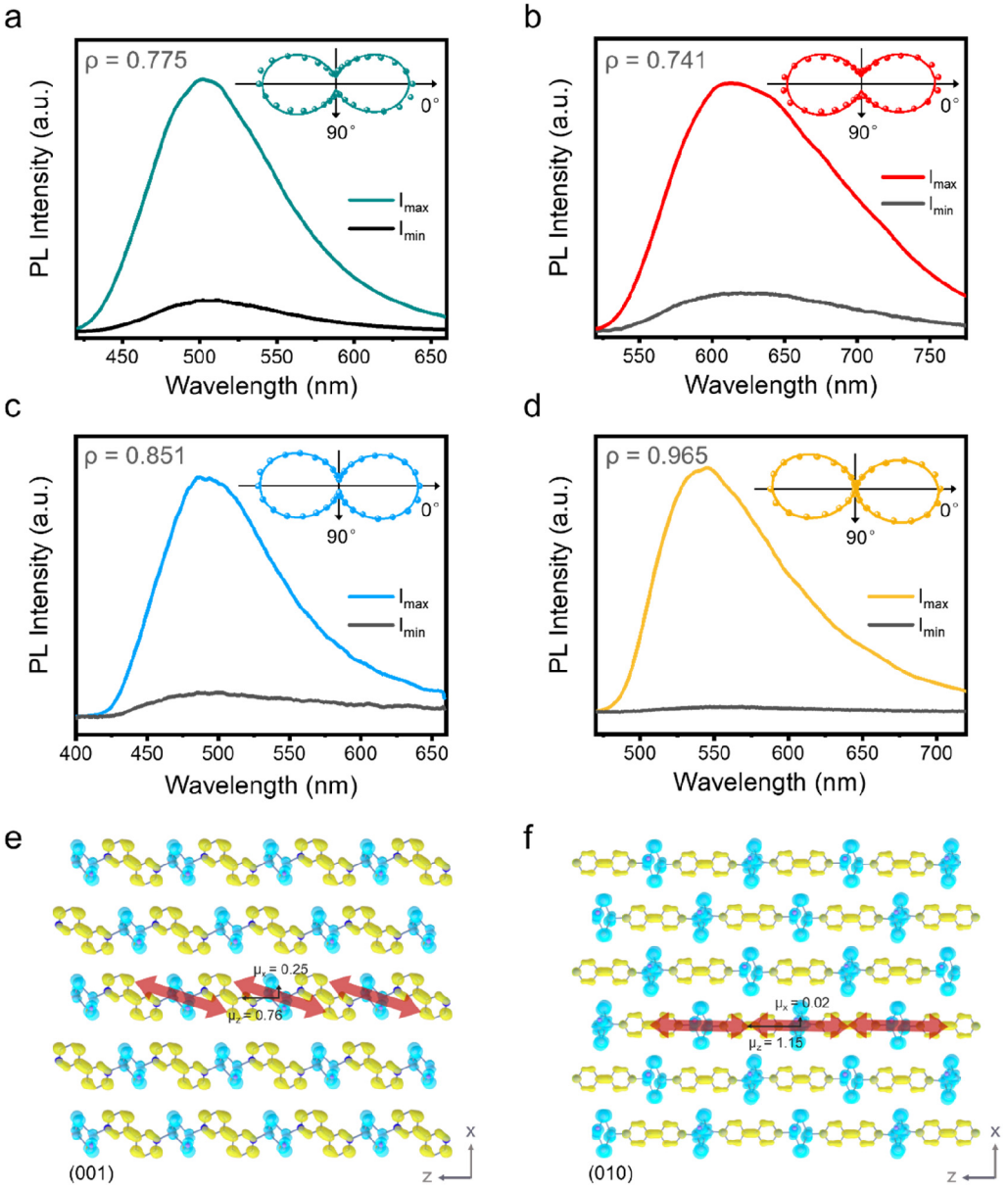

Figure 3. (a–d) PL spectra of I_{max} and I_{min} of **Cu_2I_2-pym**, **Cu_2I_2-pyz**, **Cu_2I_2-3,3′-bpy** and **Cu_2I_2-4,4′-bpy** microcrystals (λ_{ex} = 405 nm), respectively. Inset: the relevant PL polarization profile. The plotted curves are fitted with the sinusoidal function. (e) TDDFT calculated transition dipole moment distribution on (001) plane of the **Cu_2I_2-3,3′-bpy** hybrid structure. (f) TDDFT calculated transition dipole moment distribution on (010) plane of the **Cu_2I_2-4,4′-bpy** hybrid structure. The 3-methylphenyl on P-(m-Tol)$_3$ ligands are omitted for clarity.

transition dipole moments in **Cu_2I_2-3,3′-bpy** and **Cu_2I_2-4,4′-bpy** hybrid clusters are mostly aligned in the Cu-bidentate ligand quasi-2D crystal plane and maintain a highly consistent orientation, which is in line with our proposed model (Figure 1b), indicating the potential of stretched hybrid chains for the highly linear PL polarization. We further quantitatively calculated z and x components of transition dipole moments in the main exposed crystal plane of (001) and (010) for **Cu_2I_2-3,3′-bpy** and **Cu_2I_2-4,4′-bpy**, respectively. The z and x components of transition dipole moments in the **Cu_2I_2-3,3′-bpy** are 0.76 and 0.25 Debye, whereas the counterparts in the **Cu_2I_2-4,4′-bpy** are 1.15 and 0.02 Debye, respectively (Figure 3e, f). Thus, the theoretical PL polarization degree (ρ) can be estimated as 0.805 and 0.999 for the **Cu_2I_2-3,3′-bpy** and **Cu_2I_2-4,4′-bpy** hybrid structure, respectively, by using the empirical formula of $\rho = (\mu_z^2 - \mu_x^2)/(\mu_z^2 + \mu_x^2)$, where μ_z and μ_x are z and x components of the calculated transition dipole moments, respectively. These results illustrate that the near-unity light emission polarization is attributed to superalignment of the optical transition dipole moments in the **Cu_2I_2-4,4′-bpy** hybrid crystal, which is an intrinsic property of the hybrid crystal independent of excitation light (Figure S14).

To reduce the fluctuation of transition dipole moments in crystals and apply the nanoscale size effect for further improving the PL polarization degree, we synthesized hybrid nanobelts by a microemulsion approach. The Cu_4I_4[P-(m-Tol)$_3$]$_4$/chloroform and water phase microemulsion was formed with the assistance of surfactant sodium dodecyl benzenesulfonate under vigorously stirring and ultrasonication (Figure 4a). Then 4,4′-bpy ligands were added to trigger the assembly of **Cu_2I_2-4,4′-bpy** clusters under the confinement of microemulsion drops (Figure 4b). As the reaction time

https://doi.org/10.1021/acs.nanolett.1c01149
Nano Lett. 2021, 21, 4115–4121

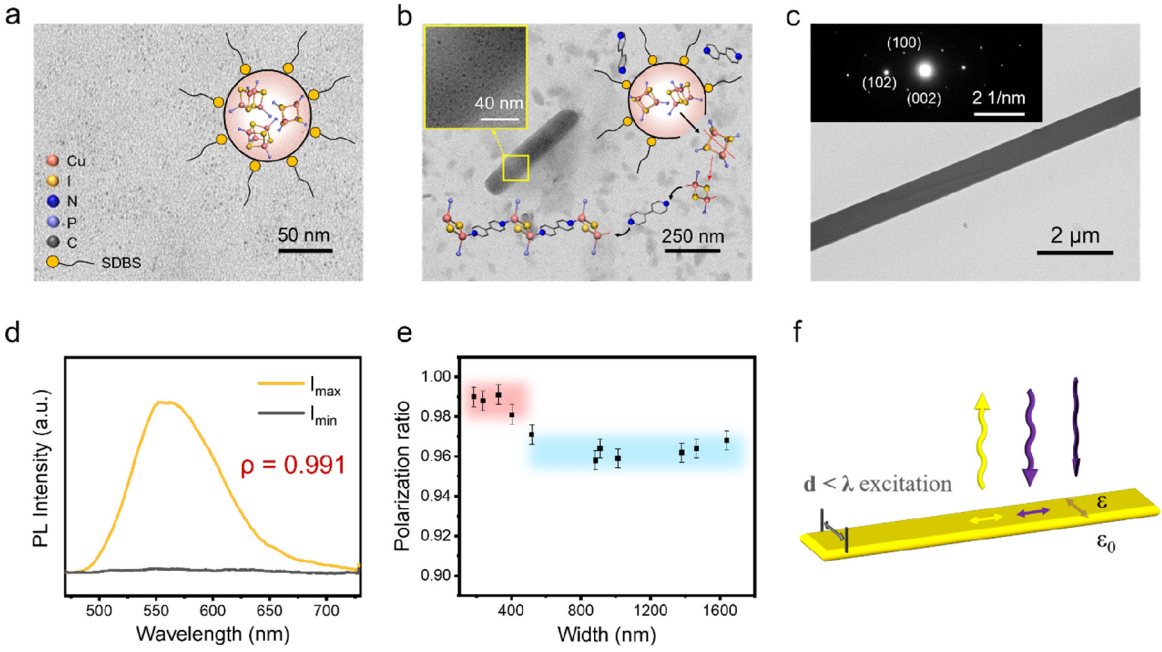

Figure 4. (a) TEM image of the formed 0D-Cu_4I_4[P-(m-Tol)$_3$]$_4$ microemulsion. Inset: schematic diagram of a microemulsion drop. (b) TEM image of small assemblies of **Cu_2I_2-4,4′-bpy** after introducing 4,4′-bpy ligand into the microemulsion system. Inset: a magnified TEM image of a preformed nanobelt (top left) and a schematic diagram of the demulsification process (top right). (c) TEM image of the finally formed nanobelt. Inset: a SAED pattern of the nanobelt. (d) PL spectra of I_{max} and I_{min} of the **Cu_2I_2-4,4′-bpy** nanobelt (λ_{ex} = 405 nm). (e) Plot of width-dependent polarization degree of **Cu_2I_2-4,4′-bpy** nanobelts. (f) Schematic diagram of the size effect in terms of the large dielectric contrast.

prolonged, the assemblies of **Cu_2I_2-4,4′-bpy** hybrid clusters spontaneously arranged periodically to form the final nanobelts (Figure 4c and Figure S15a, c) and the corresponding selected-area electron diffraction (SEAD) pattern (inset in Figure 4c) manifests their single-crystalline feature. As the control sample, **Cu_2I_2-3,3′-bpy** nanobelts were also synthesized via the similar route (Figure S15b, d). Both nanobelts display bright PL emission under the irradiation of ultraviolet light (Figure S16) and PL decay lifetimes indicating their typical phosphorescence emission (Figure S17).

We analyzed the size effect on the PL polarization degree of the obtained nanobelts. The **Cu_2I_2-4,4′-bpy** hybrid nanobelt exhibited particularly strong polarized PL emission centered at 560 nm and the polarization degree reached to 0.991 (Figure 4d), distinctly higher than that of the corresponding microcrystal (0.965). The polarized PL of a series of **Cu_2I_2-4,4′-bpy** nanobelts with different sizes were further measured (Figure S18) and the polarization degrees were correlated to the widths of the nanobelts as shown in Figure 4e. It is clear that the critical width of the **Cu_2I_2-4,4′-bpy** nanobelt for the PL polarization degree enhancement is around 400−500 nm. The **Cu_2I_2-4,4′-bpy** nanobelt with the width larger than the critical value displays the polarization degree of ∼0.96, which is the same as microcrystals. In contrast, once it is lower than the critical width, the polarization degree can reach to ∼0.99, which is the highest value among the previously reported PL materials (Table S3). The above behavior indicated an impressive role on the PL polarization degree, which is also observed in **Cu_2I_2-3,3′-bpy** nanobelts (Figures S19 and S20). Specifically, a size-effect-induced mechanism of polarization phenomenon can be described in Figure 4f. When the wavelength of light excitation is larger than the width of nanobelt, the in-plane electric field component perpendicular to the nanobelt is attenuated, which can be ascribed to a large dielectric contrast between the nanobelt (generally larger than 20 for hybrid crystals[23,24]) and its air surroundings. Meanwhile, for the direction along the nanobelt, the electric field of the electromagnetic wave is not affected. Consequently, this kind of optical antenna effect enhances the anisotropic light absorption as well as the linear polarization degree of PL. Profiting from the above results, diverse nanostructured materials with linear polarized PL could be further fabricated (Figures S21 and S22) via the proposed microemulsion approach for the application of nano-optoelectronics in future.

In summary, we have presented a crystal engineering approach based on a tunable hybrid cluster self-assembly to fabricate highly photoluminescent **Cu_2I_2-4,4′-bpy** hybrid crystals with the highest polarization degree of direct PL emission. The excellent PL polarization is driven by the highly oriented transition dipole moments in a linearly aligned direction to the full extent in quasi-2D crystal planes. Moreover, the microemulsion strategy enabled us to fabricate **Cu_2I_2-4,4′-bpy** nanobelts with introducing the size effect to realize almost completely PL polarization. Our work stresses a possibility to offer bright polarization light sources for significant optical applications such as bright three-dimensional displays, quantum information, specific bioimaging, and so forth.

■ ASSOCIATED CONTENT

Supporting Information

The Supporting Information is available free of charge at https://pubs.acs.org/doi/10.1021/acs.nanolett.1c01149.

Experimental section for material synthesis, characterization and optical measurements (PDF)

Crystallographic information files (ZIP)

https://doi.org/10.1021/acs.nanolett.1c01149
Nano Lett. 2021, 21, 4115−4121

AUTHOR INFORMATION

Corresponding Authors

Hong-Bin Yao − *Hefei National Laboratory for Physical Sciences at the Microscale and Department of Applied Chemistry, Hefei Science Center of Chinese Academy of Sciences, University of Science and Technology of China, Hefei, Anhui 230026, China;* orcid.org/0000-0002-2901-0160; Email: yhb@ustc.edu.cn

Hualing Zeng − *International Center for Quantum Design of Functional Materials (ICQD), Synergetic Innovation Center of Quantum Information and Quantum Physics, Hefei National Laboratory for Physical Sciences at the Microscale, and Key Laboratory of Strongly-Coupled Quantum Matter Physics, Chinese Academy of Sciences, Department of Physics, University of Science and Technology of China, Hefei, Anhui 230026, China;* orcid.org/0000-0001-5869-9553; Email: hlzeng@ustc.edu.cn

Guozhen Zhang − *Hefei National Laboratory for Physical Sciences at the Microscale and Department of Chemical Physics, iChEM (Collaborative Innovation Center of Chemistry for Energy Materials), University of Science and Technology of China, Hefei, Anhui 230026, China;* orcid.org/0000-0003-0125-9666; Email: guozhen@ustc.edu.cn

Authors

Jing-Jing Wang − *Hefei National Laboratory for Physical Sciences at the Microscale and Department of Applied Chemistry, Hefei Science Center of Chinese Academy of Sciences, University of Science and Technology of China, Hefei, Anhui 230026, China*

Xiaoyu Mao − *International Center for Quantum Design of Functional Materials (ICQD), Synergetic Innovation Center of Quantum Information and Quantum Physics and Key Laboratory of Strongly-Coupled Quantum Matter Physics, Chinese Academy of Sciences, Department of Physics, University of Science and Technology of China, Hefei, Anhui 230026, China*

Jun-Nan Yang − *Hefei National Laboratory for Physical Sciences at the Microscale and Department of Applied Chemistry, Hefei Science Center of Chinese Academy of Sciences, University of Science and Technology of China, Hefei, Anhui 230026, China*

Yi-Chen Yin − *Hefei National Laboratory for Physical Sciences at the Microscale and Department of Applied Chemistry, Hefei Science Center of Chinese Academy of Sciences, University of Science and Technology of China, Hefei, Anhui 230026, China*

Ji-Song Yao − *Hefei National Laboratory for Physical Sciences at the Microscale and Department of Applied Chemistry, Hefei Science Center of Chinese Academy of Sciences, University of Science and Technology of China, Hefei, Anhui 230026, China*

Li-Zhe Feng − *Hefei National Laboratory for Physical Sciences at the Microscale and Department of Applied Chemistry, Hefei Science Center of Chinese Academy of Sciences, University of Science and Technology of China, Hefei, Anhui 230026, China*

Feng Zhu − *Hefei National Laboratory for Physical Sciences at the Microscale and Department of Materials Science and Engineering, University of Science and Technology of China, Hefei, Anhui 230026, China*

Cheng Ma − *Hefei National Laboratory for Physical Sciences at the Microscale and Department of Materials Science and Engineering, University of Science and Technology of China, Hefei, Anhui 230026, China;* orcid.org/0000-0002-9761-322X

Cui Yang − *Department of Polymer Science and Engineering, University of Science and Technology of China, Hefei, Anhui 230026, China*

Gang Zou − *Department of Polymer Science and Engineering, University of Science and Technology of China, Hefei, Anhui 230026, China;* orcid.org/0000-0002-5041-5242

Complete contact information is available at: https://pubs.acs.org/10.1021/acs.nanolett.1c01149

Author Contributions

[†]J.-J.W. and X.M.contributed equally to this work.

Notes

The authors declare no competing financial interest.

ACKNOWLEDGMENTS

We acknowledge the financial support from the National Key Research and Development Program of China (Grant 2016YFA0200602, 2018YFA0208702, 2017YFA0205004, and 2018YFA0306600), the National Natural Science Foundation of China (Grant 52073271, 21875236, 21573211, 21633007, 22161142004, and 11674295), the Fundamental Research Funds for the Central Universities (Grant WK2060190085, WK2340000082, WK2030020032, and WK3510000013), the Joint Funds from Hefei National Synchrotron Radiation Laboratory (Grant KY2060000172), the State Key Laboratory of Luminescence and Applications (Grant SKLA-2020-06) and the Anhui Initiative in Quantum Information Technologies (Grant AHY090200 and AHY170000). We thank Professor Yi Luo for his helpful discussion. We also acknowledge the support from the USTC Center for Micro and Nanoscale Research and Fabrication and USTC Supercomputing Center the computing resource.

REFERENCES

(1) Wang, X. M.; Jones, A. M.; Seyler, K. L.; Tran, V.; Jia, Y. C.; Zhao, H.; Wang, H.; Yang, L.; Xu, X. D.; Xia, F. N. Highly Anisotropic and Robust Excitons in Monolayer Black Phosphorus. *Nat. Nanotechnol.* **2015**, *10* (6), 517−521.

(2) Zhu, B.; Zeng, H. L.; Dai, J. F.; Gong, Z. R.; Cui, X. D. Anomalously Robust Valley Polarization and Valley Coherence in Bilayer WS2. *Proc. Natl. Acad. Sci. U. S. A.* **2014**, *111* (32), 11606−11611.

(3) Jones, A. M.; Yu, H.; Ghimire, N. J.; Wu, S.; Aivazian, G.; Ross, J. S.; Zhao, B.; Yan, J.; Mandrus, D. G.; Xiao, D.; Yao, W.; Xu, X. Optical Generation of Excitonic Valley Coherence in Monolayer WSe_2. *Nat. Nanotechnol.* **2013**, *8* (9), 634−638.

(4) Wang, J. F.; Gudiksen, M. S.; Duan, X. F.; Cui, Y.; Lieber, C. M. Highly Polarized Photoluminescence and Photodetection from Single Indium Phosphide Nanowires. *Science* **2001**, *293* (5534), 1455−1457.

(5) Sun, M. J.; Liu, Y.; Zeng, W.; Zhao, Y. S.; Zhong, Y. W.; Yao, J. Photoluminescent Anisotropy Amplification in Polymorphic Organic Nanocrystals by Light-Harvesting Energy Transfer. *J. Am. Chem. Soc.* **2019**, *141* (15), 6157−6161.

(6) Hu, J. T.; Li, L. S.; Yang, W. D.; Manna, L.; Wang, L. W.; Alivisatos, A. P. Linearly polarized emission from colloidal semiconductor quantum rods. *Science* **2001**, *292* (5524), 2060−2063.

(7) Chamarro, M.; Gourdon, C.; Lavallard, P. Photoluminescence Polarization of Semiconductor Nanocrystals. *J. Lumin.* **1996**, *70* (1−6), 222−237.

(8) Aharonovich, I.; Englund, D.; Toth, M. Solid-state Single-photon Emitters. *Nat. Photonics* **2016**, *10* (10), 631−641.
(9) Zhang, Y. S.; Wang, S. W.; Chen, S. L.; Zhang, Q. L.; Wang, X.; Zhu, X. L.; Zhang, X. H.; Xu, X.; Yang, T. F.; He, M.; Yang, X.; Li, Z. W.; Chen, X.; Wu, M. F.; Lu, Y. R.; Ma, R. M.; Lu, W.; Pan, A. L. Wavelength-Tunable Mid-Infrared Lasing from Black Phosphorus Nanosheets. *Adv. Mater.* **2020**, *32* (17), 1808319.
(10) Lan, A. D.; Giblin, J.; Protasenko, V.; Kuno, M. Excitation and Photoluminescence Polarization Anisotropy of Single CdSe Nanowires. *Appl. Phys. Lett.* **2008**, *92* (18), 183110.
(11) Li, Y. X.; Huang, H.; Xiong, Y.; Richter, A. F.; Kershaw, S. V.; Feldmann, J.; Rogach, A. L. Using Polar Alcohols for the Direct Synthesis of Cesium Lead Halide Perovskite Nanorods with Anisotropic Emission. *ACS Nano* **2019**, *13* (7), 8237−8245.
(12) Raja, S. N.; Bekenstein, Y.; Koc, M. A.; Fischer, S.; Zhang, D. D.; Lin, L. W.; Ritchie, R. O.; Yang, P. D.; Alivisatos, A. P. Encapsulation of Perovskite Nanocrystals into Macroscale Polymer Matrices: Enhanced Stability and Polarization. *ACS Appl. Mater. Interfaces* **2016**, *8* (51), 35523−35533.
(13) Sun, Y. J.; Brandt, O.; Ramsteiner, M.; Grahn, H. T.; Ploog, K. H. Polarization anisotropy of the photoluminescence of M-plane (In,Ga)N/GaN multiple quantum wells. *Appl. Phys. Lett.* **2003**, *82* (22), 3850−3852.
(14) Hirai, Y.; Babu, S. S.; Praveen, V. K.; Yasuda, T.; Ajayaghosh, A.; Kato, T. Anisotropic Self-Assembly of Photoluminescent Oligo(p-Phenylenevinylene) Derivatives in Liquid Crystals: An Effective Strategy for the Macroscopic Alignment of p-Gels. *Adv. Mater.* **2009**, *21* (40), 4029−4033.
(15) Sakakibara, K.; Chithra, P.; Das, B.; Mori, T.; Akada, M.; Labuta, J.; Tsuruoka, T.; Maji, S.; Furumi, S.; Shrestha, L. K.; Hill, J. P.; Acharya, S.; Ariga, K.; Ajayaghosh, A. Aligned 1-D nanorods of a p-gelator exhibit molecular orientation and excitation energy transport different from entangled fiber networks. *J. Am. Chem. Soc.* **2014**, *136* (24), 8548−51.
(16) Kittikhunnatham, P.; Som, B.; Rassolov, V.; Stolte, M.; Würthner, F.; Shimizu, L. S.; Greytak, A. B. Fluorescence Polarization Measurements to Probe Alignment of a Bithiophene Dye in One-Dimensional Channels of Self-Assembled Phenylethynylene Bis-Urea Macrocycle Crystals. *J. Phys. Chem. C* **2017**, *121* (33), 18102−18109.
(17) Liu, W.; Fang, Y.; Li, J. Copper Iodide Based Hybrid Phosphors for Energy-Efficient General Lighting Technologies. *Adv. Funct. Mater.* **2018**, *28* (8), 1705593.
(18) Xie, M.; Han, C.; Zhang, J.; Xie, G.; Xu, H. White Electroluminescent Phosphine-Chelated Copper Iodide Nanoclusters. *Chem. Mater.* **2017**, *29* (16), 6606−6610.
(19) Fang, Y.; Liu, W.; Teat, S. J.; Dey, G.; Shen, Z.; An, L.; Yu, D.; Wang, L.; O'Carroll, D. M.; Li, J. A Systematic Approach to Achieving High Performance Hybrid Lighting Phosphors with Excellent Thermal- and Photostability. *Adv. Funct. Mater.* **2017**, *27* (3), 1603444.
(20) Liu, W.; Fang, Y.; Wei, G. Z.; Teat, S. J.; Xiong, K.; Hu, Z.; Lustig, W. P.; Li, J. A Family of Highly Efficient CuI-Based Lighting Phosphors Prepared by a Systematic, Bottom-up Synthetic Approach. *J. Am. Chem. Soc.* **2015**, *137* (29), 9400−8.
(21) Zhang, X.; Liu, W.; Wei, G. Z.; Banerjee, D.; Hu, Z.; Li, J. Systematic Approach in Designing Rare-Earth-Free Hybrid Semiconductor Phosphors for General Lighting Applications. *J. Am. Chem. Soc.* **2014**, *136* (40), 14230−6.
(22) Chen, C.; Li, R. H.; Zhu, B. S.; Wang, K. H.; Yao, J. S.; Yin, Y. C.; Yao, M. M.; Yao, H. B.; Yu, S. H. Highly Luminescent Inks: Aggregation-Induced Emission of Copper-Iodine Hybrid Clusters. *Angew. Chem., Int. Ed.* **2018**, *57* (24), 7106−7110.
(23) Chen, H. P.; Shi, P. P.; Wang, Z. X.; Gao, J. X.; Zhang, W. Y.; Chen, C.; Tang, Y. Y.; Fu, D. W. Tunable dielectric transitions in layered organic-inorganic hybrid perovskite-type compounds: $[NH_3(CH_2)_2Cl]_2[CdCl_{4-4x}Br_{4x}]$ (x = 0, 1/4, 1). *Dalton Trans.* **2018**, *47* (20), 7005−7012.
(24) Wei, W. J.; Li, C.; Li, L. S.; Tang, Y. Z.; Jiang, X. X.; Lin, Z. S. Phase transition, optical and dielectric properties regulated by anion-substitution in a homologous series of 2D hybrid organic-inorganic perovskites. *J. Mater. Chem. C* **2019**, *7* (38), 11964−11971.

https://doi.org/10.1021/acs.nanolett.1c01149
Nano Lett. 2021, 21, 4115−4121